Zeyin He ✉
Weiyi Tang
Shizheng Sun

https://doi.org/10.21278/TOF.452021720
ISSN 1333-1124
eISSN 1849-1391

A MODEL FOR ANALYSIS OF TIME-VARYING MESH STIFFNESS OF HELICAL GEARS WITH MISALIGNMENT ERRORS

Summary

A mathematical model is proposed to calculate the time-varying mesh stiffness (TVMS) of helical gears under the condition of gear misalignment by combining the slice method. The proposed method aims to reveal the influences of different misalignment errors (centre distance error, action plane error and off action plane error) on the TVMS of helical gears. The results show that the misalignment error on the plane of action has an enormous influence on mesh characteristics and that it not only changes the contact line and load distribution but also results in a reduced TVMS. Meanwhile, the centre distance error causes the amplitude fluctuation of TVMS and transmission error (TE). The misalignment error on the off plane of action has almost no effect on TVMS and TE. The results can be used for vibration prediction and misalignment fault diagnosis.

Key words: *time-varying mesh stiffness; misalignment errors; helical gears; slice method*

1. Introduction

Time-varying mesh stiffness (TVMS) is one of the most important dynamic excitations of a gear system, and it is a significant parameter for calculating vibration and noise of the gear system. In a practical application process, assembly error, manufacture error and elastic deformation always cause misalignment errors, which could change the mesh characteristic of gear pairs. Therefore, determining the influences of misalignment errors on the TVMS is valuable for the diagnosis of mechanical vibration faults.

Relevant studies have been made to investigate the relationships between mesh characteristics and misalignment errors. A method for the calculation of load distributions with manufacturing and misalignment errors of gears is developed by Simon [1]. Then, the influence of misalignment and tooth profile error on the contact pressure distribution of spiral bevel gear is studied [2]. Kahraman [3] developed a nonlinear time-varying dynamics model of planetary gear sets considering manufacturing errors and assembly errors and studied the load distribution characteristics. The influence of the misalignment error on other mesh characteristics of gears has also been studied. Hu [4] set up a test rig for a polymer gear to investigate wear performance of acetal gears with misalignment. Kumar [5] studied the gear tooth effective contact area with different misalignment errors. It was shown that the misalignment error would reduce the contact area.

Finite element method (FEM) is one of the effective methods to analyse mesh characteristics of gear pairs. Li [6, 7] developed a FEM to quantitatively investigate the mesh characteristics of a spur gear pair with misalignment errors. It was found that the TVMS of a spur gear pair with misalignment errors becomes high with an increase in torque load. Our group [8] proposed a FEM to study the TE of a helical gear system with machining errors, assembly errors and tooth modifications.

The analytical method of mesh stiffness calculation has higher computational efficiency than the experimental method and the FEM. Feng [9] proposed an analytical method to calculate the TVMS of healthy helical gears based on the slice method. Wan [10] used an accumulated integral potential energy method to calculate the healthy helical gear mesh stiffness. Wang [11] calculated the TVMS of healthy helical gears with an axial mesh force component. For helical gear pairs with errors, many scholars focused mainly on the TVMS with tooth crack [12,13] and tooth spalling [14,15], and discussed the relationships between mesh stiffness and different crack or spalling parameters. However, there are few studies on the TVMS analysis with mesh misalignment errors based on the slice method and the relationship between the TVMS and coupling misalignment errors.

Therefore, a mathematical model is proposed to calculate the TVMS with misalignment errors, and a misalignment error model of a parallel shaft gear system is built. The effects of centre distance, misalignment error on the plane of action and off plane of action are considered and variations of mesh stiffness are analysed.

2. Contact line of helical gears

There is a difference in contact line between helical gears and spur gears with respect to the helix angle. The contact ratio of a helical gear includes transverse contact ratio ε_α and axial contact ratio ε_β, according to their sizes, and it is divided into $\varepsilon_\alpha \geq \varepsilon_\beta$ and $\varepsilon_\alpha < \varepsilon_\beta$. In general, ε_α is greater than ε_β, so in this paper, we take the case $\varepsilon_\alpha \geq \varepsilon_\beta$ as an example as it is more common in the engineering application. The action plane of helical gear $A_0B_0C_0D_0$ is shown in Fig. 1, the length of A_0B_0 is face width B, the length of B_0C_0 is equal to the transverse practical line of action, and B_0B_5 denotes the distance through which the helical gear moves along the base cylinder during meshing. The angle between contact line and tooth width direction is the helix angle on base cylinder β_b, so the maximum length of the contact line can be expressed as:

$$L_{max} = B / \cos\beta_b \tag{1}$$

According to Fig. 1, during the meshing process, the tooth starts meshing at point B_0 and finishes meshing at point B_5, and the contact line of the gear teeth gradually shifts from point B_0 to point B_5. Therefore, the length of a single tooth contact line is represented as a function of the meshing time t

$$L(t) = \begin{cases} L_{\max} t / (\varepsilon_\beta t_z) & t \in [\ 0\ , \varepsilon_\beta t_z] \\ L_{\max} & t \in [\varepsilon_\beta t_z, \varepsilon_\alpha t_z] \\ L_{\max}(\varepsilon_\gamma t_z - t) / (\varepsilon_\beta t_z) & t \in [\varepsilon_\alpha t_z, \varepsilon_\gamma t_z] \end{cases} \tag{2}$$

where $t_z = p_{bt} / \omega r_b$ denotes the time of the gear moving along the line of action, p_{bt} is the base pitch at transverse section, ω denotes the gear angular velocity, r_b denotes the radius of the basis circle, and $\varepsilon_\gamma = \varepsilon_\alpha + \varepsilon_\beta$ denotes the gear total contact ratio of the helical gear.

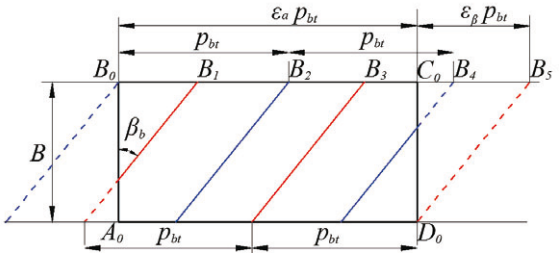

Fig. 1 Action plane of a helical gear

Because of the non-integer of the helical gears' contact ratio, there are several contact lines in the plane of action at the same time. The transverse distance between the two adjacent contact lines is equal to p_{bt}, which means, there is multi-tooth meshing during engagement. The number of teeth engaged changes with meshing time, presenting the phenomenon of multi-tooth meshing with less-tooth meshing alternately. Segments B_0-B_1, B_2-B_3 and B_4-B_5 represent multi-tooth meshing, and segments B_1-B_2 and B_3-B_4 represent less-tooth meshing.

The length of total contact lines is the sum of the contact line length of each pair. Due to the phenomenon of multi-tooth meshing, the length of the total contact line changes over time which can be expressed as a function of time t as follows:

$$L_{total}(t) = \sum_{i=1}^{M} L_i(t) \tag{3}$$

where M is the number of teeth which participate in meshing simultaneously.

3. Mesh misalignment of helical gears

Fig. 2 shows a coordinate system in which gear mesh misalignment errors are defined. For a pair of parallel shaft helical gears, take the centre axis of each helical gear as z axis to establish two three-dimensional coordinate systems (O_1–$x_1y_1z_1$, O_2–$x_2y_2z_2$). Where O_1O_1 and O_2O_2 represent the shaft of a normal pinion and gear, respectively, these two axes are parallel to each other, and the distance between the two axes is equal to the standard centre distance. Plane I is defined as an axis plane which is formed by two axes, and plane II is perpendicular to plane I. O_1O_1' is the new position of O_1O_1 with gear mesh misalignment, the misalignment errors of O_1O_1' on two planes are expressed as θ_x and θ_y respectively, and the misalignment error on the centre distance is expressed as $\pm\Delta a$, where "+" represents an increase in the centre distance, and "-" denotes a decrease in the centre distance.

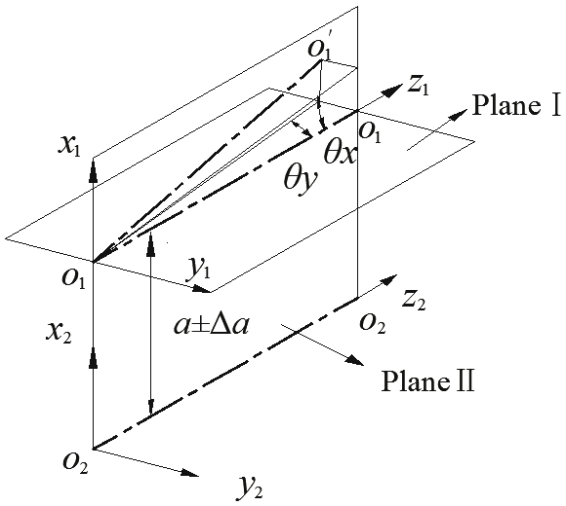

Fig. 2 Schematic diagram of mesh misalignment errors

To more conveniently characterise the influence of misalignment errors on the meshing characteristics, a new coordinate system as shown in Fig. 3 is established, which is called the meshing plane coordinate system. The misalignment error on the plane of action (*POA*) is defined as θ_{POA}, the off plane of action (*OPOA*) is vertical to the *POA*, and the misalignment error on the O*POA* is defined as θ_{OPOA} (see Fig. 4). Misalignment errors θ_x and θ_y are converted to θ_{POA} and θ_{OPOA}, which can be expressed as

$$\begin{cases} \theta_{POA} = \arctan(\tan\theta_y \sin\alpha_n + \tan\theta_x \cos\alpha_n) \\ \theta_{OPOA} = \arctan(\tan\theta_y \cos\alpha_n + \tan\theta_x \sin\alpha_n) \end{cases} \tag{4}$$

where α_n denotes the normal pressure angle.

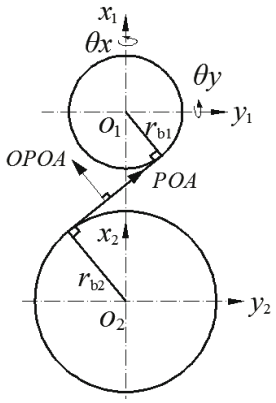

Fig. 3 Meshing plane coordinate system

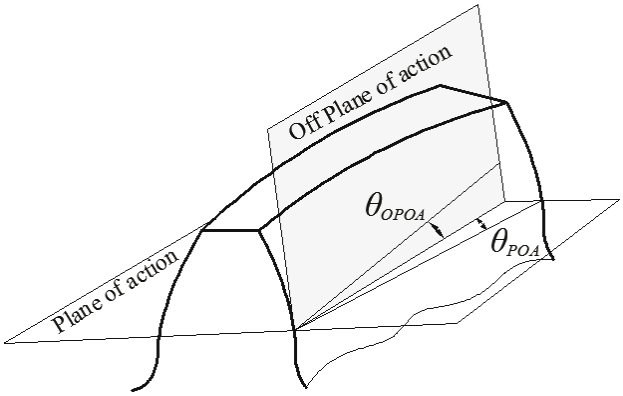

Fig. 4 Schematic diagram of θ_{POA} and θ_{OPOA}

3.1 Centre distance error

In normal conditions, two reference circles of gears are tangent, and the transverse pressure angle of the reference circle is equal to the meshing angle. The centre distance error acts along plane I, and it will change the centre distance. The pitch radius of the two gears is no longer equal to the reference radius, and the transverse pressure angle with a centre distance error is expressed as:

$$\alpha_t' = ar\cos(a\cos\alpha_t / a') \tag{5}$$

where a' is the actual centre distance with a centre error, $a' = a \pm \triangle a$.

A change in the centre distance will change the transverse contact ratio and affect the tooth contact area. The transverse contact ratio with a centre distance error can be obtained as:

$$\varepsilon_a' = \frac{1}{2\pi}[z_1(\tan\alpha_{at1} - \tan\alpha_t') + z_2(\tan\alpha_{at2} - \tan\alpha_t')] \tag{6}$$

where α_{at1} and α_{at2} denote the transverse pressure angles of the addendum circle for pinion and gear, and z_1 and z_2 represent the tooth number of pinion and gear, respectively.

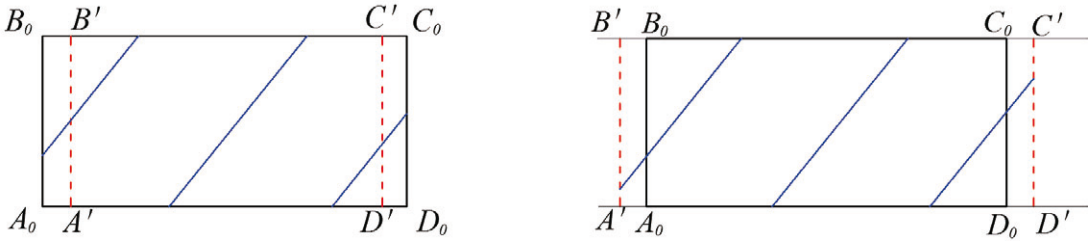

(a) Increase in centre distance (b) Decrease in centre distance

Fig. 5 Action plane with a centre distance error

Fig. 5 shows the action plane with a centre distance error. The gear action plane $A_0B_0C_0D_0$ changes to $A'B'C'D'$ because of a change in the transverse contact ratio, and the length of $B'C'$ decreases with an increase in the centre distance. On the contrary, the length of $B'C'$ increases when the centre distance becomes smaller.

The length of the contact line with a centre distance error is

$$L'(t)=\begin{cases} L_{\max}t/(\varepsilon_\beta t_z) & t\in[\ 0\ ,\varepsilon_\beta t_z] \\ L_{\max} & t\in[\varepsilon_\beta t_z,\varepsilon'_\alpha t_z] \\ L_{\max}(\varepsilon'_\gamma t_z-t)/(\varepsilon_\beta t_z) & t\in[\varepsilon'_\alpha t_z,\varepsilon'_\gamma t_z] \end{cases} \tag{7}$$

3.2 Misalignment error on the plane of action

A misalignment error on the plane of action will result in an uneven displacement gap in the direction of tooth width. Fig 6. shows a schematic diagram of tooth load with $\theta_{POA,}$ the load distribution on the tooth surface is no longer uniformly distributed along the contact line, and an edge contact occurs at one end of the tooth width. The cubic parabola law shown in Fig. 7 can reflect the load distribution on the tooth surface.

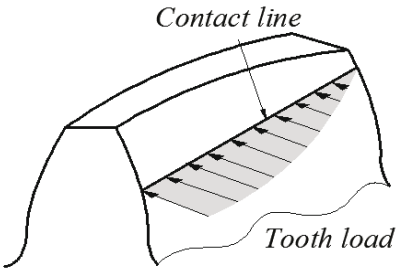

Fig. 6 Schematic diagram of tooth load

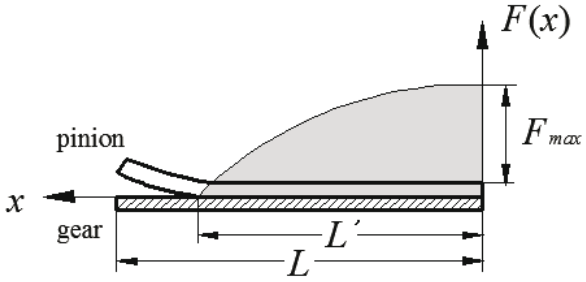

Fig. 7 Load distribution with θ_{POA}

The load of the unit tooth width at x of the tooth width can be expressed as:

$$F(x)=F_{\max}[1-(\frac{x}{L'})^3] \tag{8}$$

where $F_{\max}$ denotes the maximum load, L' is the length of the actual contact line.
The tangential load on the gear width can be defined as follows:

$$F=\int_0^{L'}F(x)\mathrm{d}x=\frac{3}{4}L'F_{\max} \tag{9}$$

The maximum load of the tooth width can be expressed as:

$$F_{\max}=C_\gamma e_m\frac{L'}{L} \tag{10}$$

where C_γ denotes the spring constant and e_m is the error on the plane of action. According to Eq. (8) to Eq.(10), the length of the actual contact line can be deduced as:

$$L'=\sqrt{\frac{4FL}{3C_\gamma e_m}} \tag{11}$$

3.3 Misalignment error on the off plane of action

A misalignment error on the off plane of action can result in the shape of the contact area to be slightly skewed, and the influence of the slight skew on the contact area is small

which can be neglected for simplicity. In this paper, it is assumed that the contact area shape does not change, and a slight decrease in the helical angle on the base cylinder is used to replace the action plane slight skew caused by the misalignment error on the off plane of action (see Fig. 8).

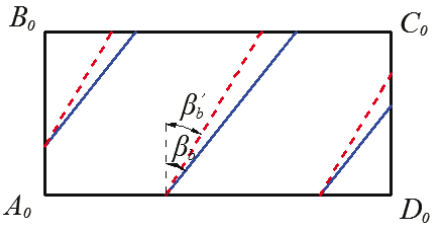

Fig. 8 Action plane with misalignment error θ_{OPOA}

The normal helix angle on the base cylinder β_b should be substituted by β_b', which is calculated by using Eq. (12)

$$\beta_b' = \beta_b - \theta_{OPOA} \tag{12}$$

4. Time-varying mesh stiffness with misalignment errors

The spur gear stiffness algorithm cannot be directly applied to the helical gear. The spur gear can be seen as a helical gear with a helix angle of zero. In Fig. 9, the helical gear is composed of a range of independent slices with a smaller thickness along the tooth width direction. These slices are a series of spur gears with a certain rotation angle, and each slice width is dl. Then the mesh stiffness of the helical gear can be obtained by calculating the mesh stiffness of the slices.

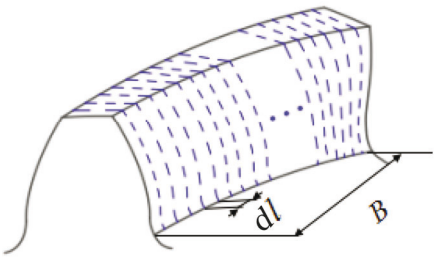

Fig. 9 Schematic of the tooth slice method

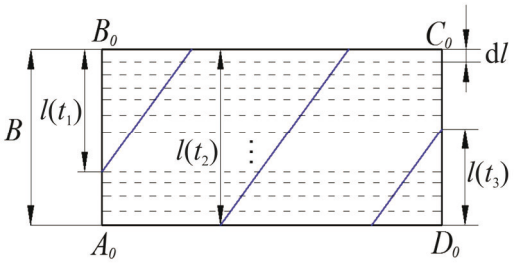

Fig. 10 (b) Slice on plane of action

Similarly, the action plane can be broken into some thin planes whose thickness is dl (see Fig. 10). The effective contact face width of gear meshing is expressed in l, which can be expressed as:

$$l(t) = L(t)\cos\beta_b \tag{13}$$

Obviously, the mesh point of each slice is not at the same place because the helix angle and the pressure angle of each slice are not the same either. $\alpha_{1i,j}$ is assumed as the linear change and it can be obtained by

$$\alpha_{1i,p} = \alpha_{1,p}(t) - [\alpha_{1,p}(\varepsilon_\beta t_z) - \alpha_{1,p}(0)]i / N \tag{14}$$

$$\alpha_{1i,g} = \alpha_{1,g}(t) + [\alpha_{1,g}(0) - \alpha_{1,g}(\varepsilon_\beta t_z)]i / N \tag{15}$$

where i is the number of spur gear slices, and subscripts "p" and "g" denote pinion and gear, respectively, while N denotes the total number of spur gear slices.

Fig. 11 is a TVMS solution model of a spur slice. The spur gear slice is considered as a variable section cantilever beam on the base cylinder. Based on the potential energy method, Hertzian energy dU_h, bending energy dU_b, shear energy dU_s and axial compressive energy dU_a can be obtained by:

$$\mathrm{d}U_h = \frac{F^2}{2\mathrm{d}k_h} \tag{16}$$

$$\mathrm{d}U_b = \frac{F^2}{2\mathrm{d}k_b} = \int_0^d \frac{[F_b(d-x) - F_a h]^2}{2EI_x}\mathrm{d}x \tag{17}$$

$$\mathrm{d}U_s = \frac{F^2}{2\mathrm{d}k_s} = \int_0^d \frac{1.2F_b^{\,2}}{2GA_x}\mathrm{d}x \tag{18}$$

$$\mathrm{d}U_a = \frac{F^2}{2\mathrm{d}k_a} = \int_0^d \frac{F_a^{\,2}}{2EA_x}\mathrm{d}x \tag{19}$$

where F is the action force, F_a and F_b are the radial and the tangential force of the action force. G and E denote shear modulus and Young's modulus. d is the distance between the mesh point and the base circle. dA_x and dI_x represent the area and the moment of inertia of the slice section where the distance to the base circle is x, which can be calculated by:

$$\mathrm{d}I_x = \frac{2h_x^{\,3}\mathrm{d}l}{3} \tag{20}$$

$$\mathrm{d}A_x = 2h_x\mathrm{d}l \tag{21}$$

where h_x denotes the height of the slice where the distance to the tooth root is x.

From Eq. (16) to Eq. (21), Hertzian stiffness dk_h, bending stiffness dk_b, shear stiffness dk_s and axial compressive stiffness dk_a of the spur gear slice can be deduced as follows:

$$\mathrm{d}k_h = \frac{\pi E\mathrm{d}l}{4(1-\nu^2)} \tag{22}$$

$$\frac{1}{\mathrm{d}k_b} = \int_{-\alpha_{1i}}^{\alpha_2} \frac{3\{1+\cos\alpha_{1i}[(\alpha_2-\alpha)\sin\alpha - \cos\alpha]\}^2(\alpha_2-\alpha)\cos\alpha}{2E\mathrm{d}l[\sin\alpha + (\alpha_2-\alpha)\cos\alpha]^3}\mathrm{d}\alpha \tag{23}$$

$$\frac{1}{\mathrm{d}k_s} = \int_{-\alpha_{1i}}^{\alpha_2} \frac{1.2(1+\nu)(\alpha_2-\alpha)\cos\alpha\cos^2\alpha_{1i}}{E\mathrm{d}l[\sin\alpha + (\alpha_2-\alpha)\cos\alpha]}\mathrm{d}\alpha \tag{24}$$

$$\frac{1}{\mathrm{d}k_a} = \int_{-\alpha_{1i}}^{\alpha_2} \frac{(\alpha_2-\alpha)\cos\alpha\sin^2\alpha_{1i}}{2E\mathrm{d}l[\sin\alpha + (\alpha_2-\alpha)\cos\alpha]}\mathrm{d}\alpha \tag{25}$$

where ν denotes Poisson's ratio.

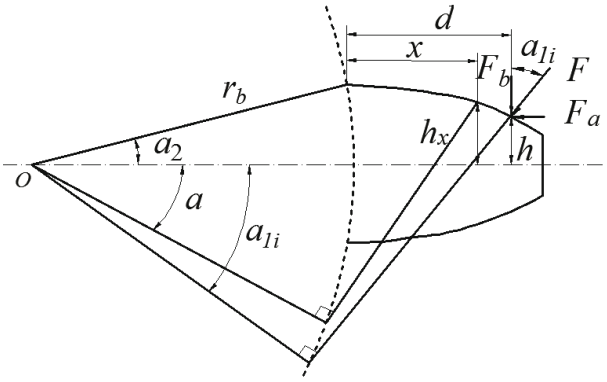

Fig. 11 Mesh stiffness solution model of a spur slice

Consequently, mesh stiffness of the helical gear can be derived by summing all values of mesh stiffness of all slices.

$$k_b = \sum_{i=1}^{N} \frac{1}{\int_{-\alpha_{1i}}^{\alpha_2} \frac{3\{1+\cos\alpha_{1i}[(\alpha_2-\alpha)\sin\alpha-\cos\alpha]\}^2(\alpha_2-\alpha)\cos\alpha}{2E[\sin\alpha+(\alpha_2-\alpha)\cos\alpha]^3}\mathrm{d}\alpha}\Delta y \tag{26}$$

$$k_s = \sum_{i=1}^{N} \frac{1}{\int_{-\alpha_{1i}}^{\alpha_2} \frac{1.2(1+\nu)(\alpha_2-\alpha)\cos\alpha\cos^2\alpha_{1i}}{E[\sin\alpha+(\alpha_2-\alpha)\cos\alpha]}\mathrm{d}\alpha}\Delta y \tag{27}$$

$$k_a = \sum_{i=1}^{N} \frac{1}{\int_{-\alpha_{1i}}^{\alpha_2} \frac{(\alpha_2-\alpha)\cos\alpha\sin^2\alpha_{1i}}{2E[\sin\alpha+(\alpha_2-\alpha)\cos\alpha]}\mathrm{d}\alpha}\Delta y \tag{28}$$

where $\Delta y = l/N$.

In addition, the foundation stiffness of the gear also needs to be taken into account [16], which can be found by using Eq. (29).

$$\frac{1}{k_f} = \frac{\cos^2\alpha_{1i}}{EL}\{L^*(\frac{u_f}{S_f})^2 + M^*(\frac{u_f}{S_f}) + P^*(1+Q^*\tan^2\alpha_{1i})\} \tag{29}$$

where u_f, S_f, L^*, M^*, P^* and Q^* can be found in Ref. [13]

Therefore, the mesh stiffness of the helical gear includes Hertzian, bending, shear, axial compressive and foundation stiffness, and the single-tooth-pair mesh stiffness of helical gear k_1 can be given by:

$$k_1 = \frac{1}{\frac{1}{k_h}+\frac{1}{k_{b1}}+\frac{1}{k_{s1}}+\frac{1}{k_{a1}}+\frac{1}{k_{f1}}+\frac{1}{k_{b2}}+\frac{1}{k_{s2}}+\frac{1}{k_{a2}}+\frac{1}{k_{f2}}} \tag{30}$$

where subscripts “1” and “2” denote pinion and gear, respectively.

In the process of meshing, there are several pairs of gear teeth meshing simultaneously. The TVMS of helical gears is the sum of the values of mesh stiffness which participate in meshing, and it is expressed as Eq. (31). A flow chart of the TVMS calculation process with misalignment errors is presented in Fig. 12.

$$K = \sum_{n=1}^{M} k_n \tag{31}$$

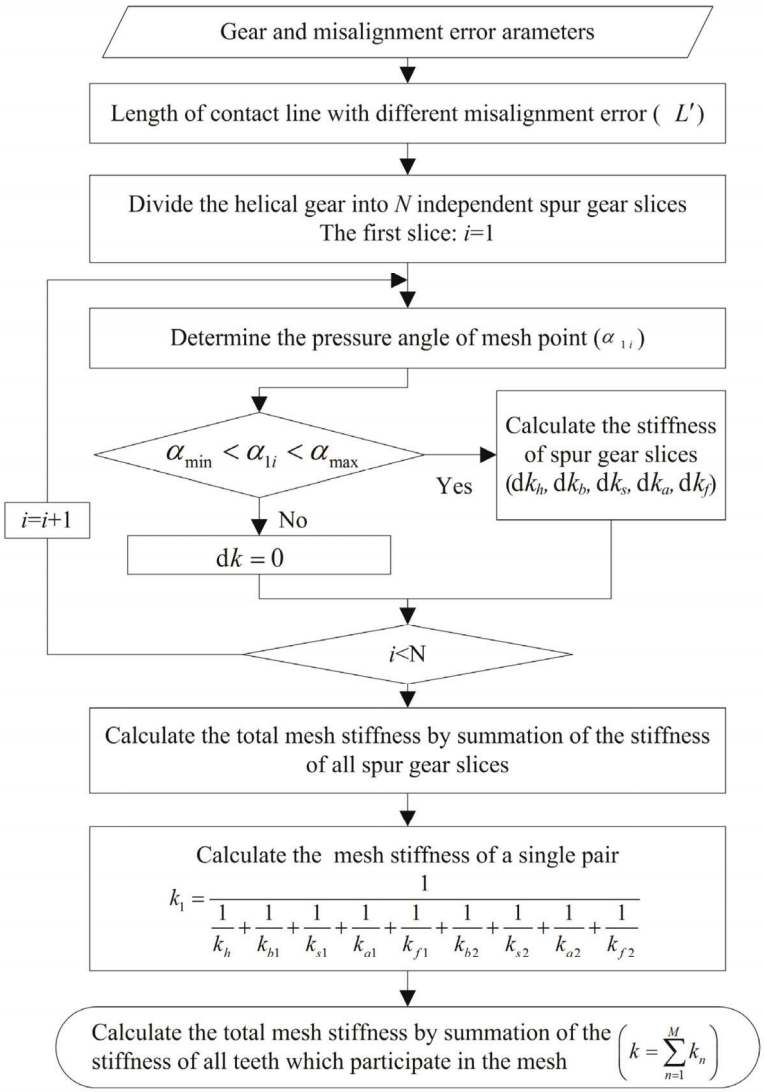

Fig. 12 Flow chart of TVMS calculation with misalignment errors

5. Results and discussion

The main parameters of the helical gear pair are listed in Table 1. The length of a single tooth is shown in Fig. 13(a). From the initial contact to the end of engagement the length of a single tooth contact line increases with time, then it remains unchanged, and finally decreases to zero at the end of meshing. Fig. 13(b) shows the variation of the total contact line length, i.e. the total contact line length exhibits a periodic variation, which is consistent with the multi-tooth alternate meshing phenomenon.

Table 1 Parameters of helical gears

Parameters	Pinion	Gear
Number of teeth z	19	49
Normal module m_n /mm	8	
Pressure angle α_n /deg	20	
Helix angle β /deg	25	
Face width B /mm	75	
Young's modulus E /GPa	210	
Poisson's ratio ν	0.3	

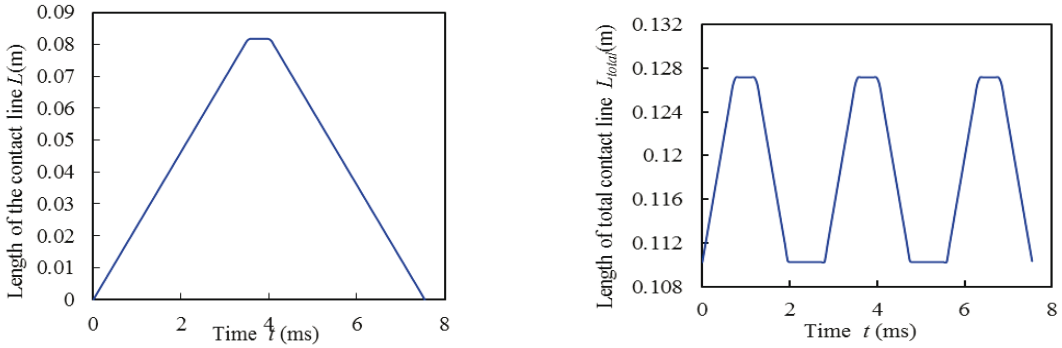

(a) Single tooth contact line (b) Total contact line

Fig. 13 Contact line length

Fig. 14 presents the TVMS curve of a healthy helical gear pair. TVMS is similar to the variation law of the total length of contact line and presents periodic changes due to the alternating meshing pattern between three teeth and two teeth. The meshing stiffness has no step-type abrupt change because the length of the contact line changes gradually, which is one of the reasons why the helical gear is more stable than the spur gear. The TE of the healthy helical gear is plotted in Fig. 15, which shows that the variation law of the TE is opposite to the TVMS curve, and the TE is smaller in the three-tooth meshing area and larger in the two-tooth meshing area.

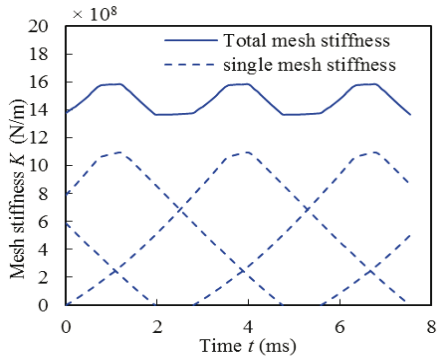

Fig. 14 TVMS of a healthy helical gear

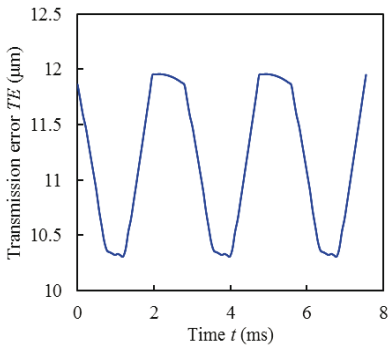

Fig. 15 Transmission error of a healthy helical gear

The length of the contact line with centre distance errors Δa=±0.15mm is shown in Fig. 16. It can be seen that the time of exit engagement has changed by the centre distance error. This is because centre distance errors change the contact ratio, and the time of exit engagement extends with increases in the contact ratio.

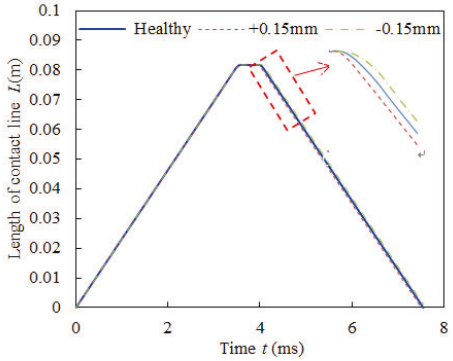

Fig. 16 Length of the contact line with a centre distance error

In order to facilitate a better observation of the influence of misalignment errors on the time-varying mesh stiffness, the time-domain coordinates of the results are dimensionless with the mesh cycle. The values of the TVMS obtained from the developed method with centre distance error Δa=±0.1, 0.15mm are given in Fig 17. Fig. 18 shows the relationships between the transmission error value and the centre distance error. It is shown that the centre distance error causes the amplitude fluctuation of TVMS and TE, the TVMS becomes higher when the gear centre distance increases, and the TE is reduced when the gear centre distance increases. In the case of a decrease, the amplitudes of the TE become smaller than in the case of the healthy gear pair. This is because the gear meshing contact area has been changed by the centre distance error. When the centre distance becomes larger, the meshing contact area decreases, the load becomes larger under the unit meshing area, and the deformation becomes larger. On the contrary, when the centre distance decreases, the meshing contact area increases, the load under the unit meshing area decreases, and the deformation is increased.

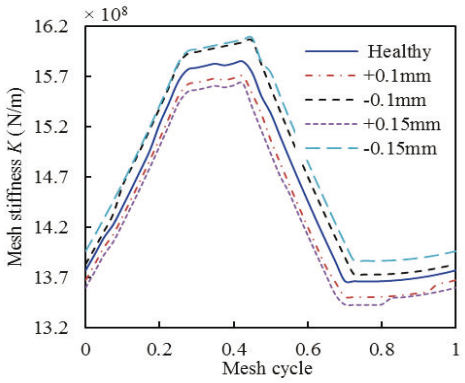

Fig. 17 TVMS with different centre distance errors

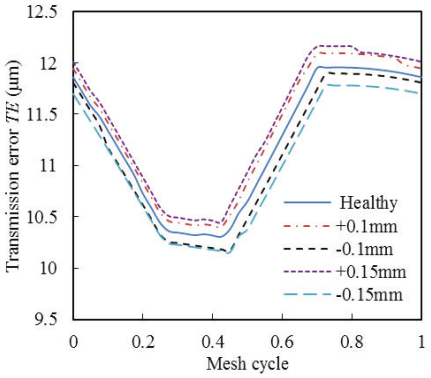

Fig. 18 TE with different centre distance errors

Fig. 19 shows load distribution of a pair of gears from the start of meshing to the end of meshing, where each line represents the instant contact line for a certain angular position of the pinion. It shows that the gear axis has a certain angle with the contact line of helical gear, and their length is time-varying. As shown in Fig. 19(a), the tooth surface load of the healthy gear is evenly distributed on the contact line, it gradually increases to the maximum in the middle of the meshing with the meshing time, and then decreases gradually with some part of the gear teeth out of meshing. Fig. 19(b) shows load distribution with misalignment error θ_{POA}=0.02°. According to the analysis of the results, the tooth load distribution of the contact line with misalignment errors on the action plane is uneven, causing an eccentric load phenomenon, in which the load on one end of the gear tooth is significantly higher than at the other end and the maximum tooth load becomes larger than in the case of the healthy gear pair.

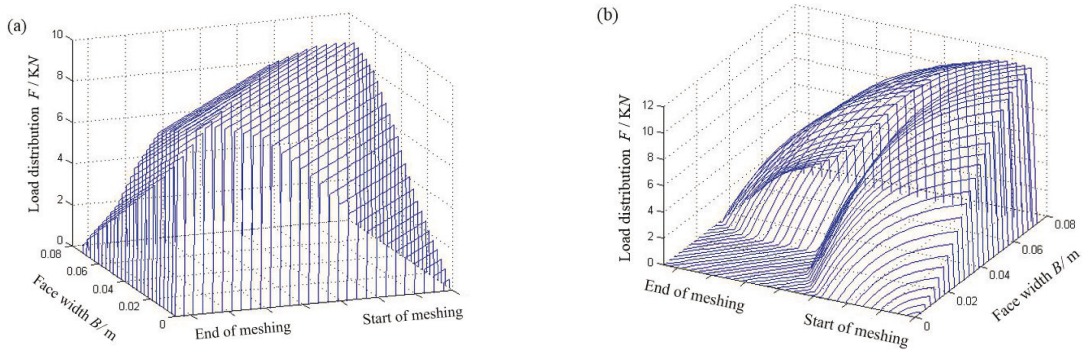

(a) Healthy gear

(b) $\theta_{POA} = 0.02^{\circ}$

Fig. 19 Load distribution

Fig. 20 presents a comparison of the length of the helical gear contact line between the healthy gear and θ_{POA}=0.01°, 0.02°, 0.03°. It is found that the length of the contact line in the middle of meshing becomes smaller and smaller gradually with the misalignment error increasing. It reveals that θ_{POA} causes a partial contact, and this phenomenon becomes more serious with an increase in the misalignment error angle.

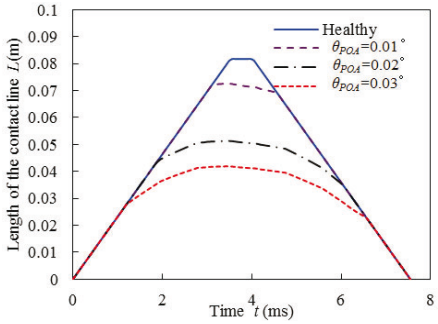

Fig. 20 Length of the contact line with θ_{POA}

Fig. 21 shows a change in TVMS with misalignment error θ_{POA}, and the TVMS decreases substantially with an increase of θ_{POA}. The transmission error refers to the motion error caused by tooth deformation, gear assembly error and manufacturing error. This paper uses the proposed mesh stiffness mathematical model to obtain the tooth deformation. Then the misalignment error on the plane of action θ_{POA} is used to obtain a gear gap on the meshing plane, and finally the two are combined to obtain the transmission error of the gear pair with the θ_{POA}. The transmission errors with θ_{POA} are shown in Fig. 22, which shows that misalignment error θ_{POA} causes the TE of the gear to become larger.

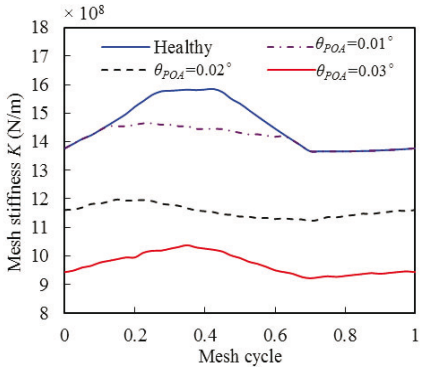

Fig. 21 TVMS with different θ_{POA}

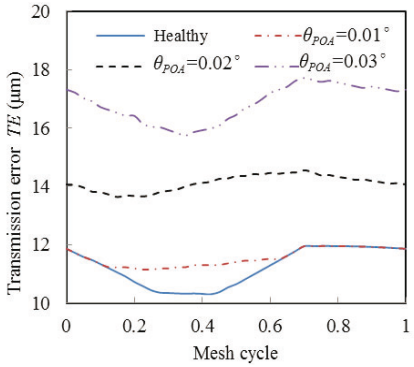

Fig. 22 TE with different θ_{POA}

TVMS and TE of the gear with misalignment errors θ_{OPOA}=0.1° and 0.2° are calculated separately too; here θ_{OPOA} is greater than θ_{POA}. It can be seen in Figs 23 and 24 that θ_{OPOA} has almost no effect on TVMS and TE. The slight skew of the action plane has little effect on the tooth contact.

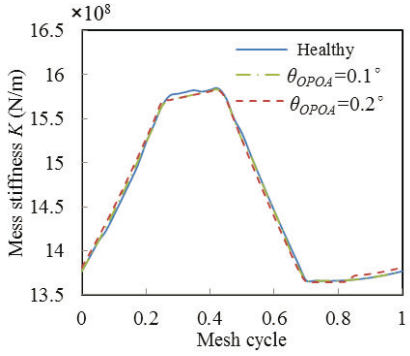

Fig. 23 TVMS with different θ_{OPOA}

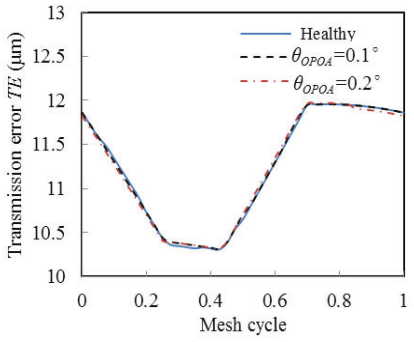

Fig. 24 TE with different θ_{OPOA}

However, in practice, there are usually multiple errors, i.e. Δa and θ_{POA}, Δa and θ_{OPOA}, θ_{OPOA} and θ_{POA}, Δa and θ_{OPOA} and θ_{POA}. In this study, we assume the misalignment errors to be Δa=+0.15 mm, θ_{POA}=0.02°, θ_{OPOA}=0.1°. Based on the orthogonal design, the case of multiple errors is shown in Table 2.

Table 2 Case of multiple errors

	Centre distance error Δa /mm	Misalignment error θ_{POA} /°	Misalignment error θ_{OPOA} /°
Case1	+0.15	0.02	0
Case2	+0.15	0	0.1
Case3	0	0.02	0.1
Case4	+0.15	0.02	0.1

As shown in Fig. 25, the TMVS of each case is calculated, and it is found that the meshing stiffness is the most sensitive to θ_{POA} and the least sensitive to θ_{OPOA}, and the centre distance error has little influence on TVMS. Therefore, error θ_{POA} should be reduced to ensure meshing performance.

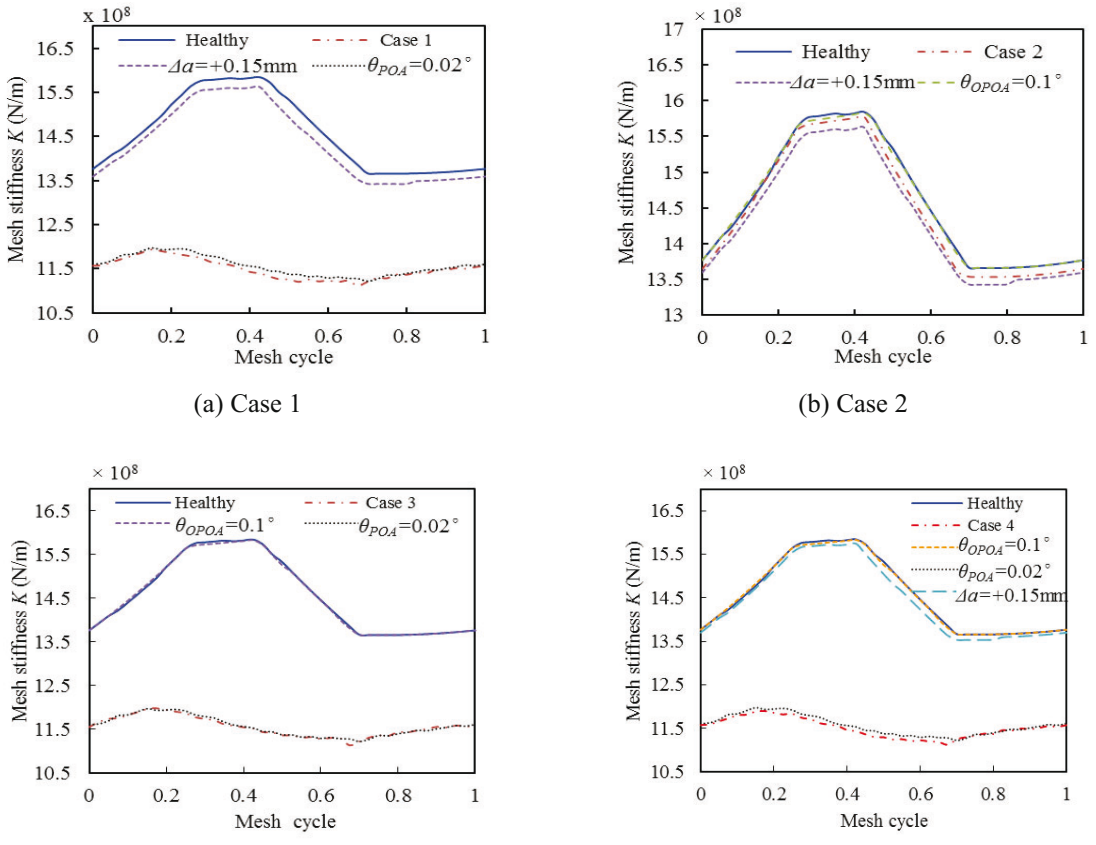

Fig. 25 Different cases of TVMS

6. Conclusions

A mathematical model is presented to evaluate TVMS of helical gears considering misalignment errors that include θ_{POA}, θ_{OPOA} and Δa. Then, the relationships between the TVMS and multiple misalignment errors are studied. The conclusions are summarized as follows:

(1) The research results show that misalignment error θ_{POA} has a considerable influence on TVMS, and that mesh stiffness is reduced with the error angle increasing. It causes eccentric load on the tooth side, and the maximum tooth load becomes greater than in healthy pairs.

(2) The centre distance error causes the amplitude fluctuation of TVMS and TE, and the TVMS decreases with an increase in the centre distance, and increases with a decrease in the centre distance. The change law of TE is opposite to mesh stiffness.

(3) Four cases of multiple error conditions are established to explore the actual situation. It is found that meshing stiffness is the most sensitive to θ_{POA} and the least sensitive to θ_{OPOA}.

Acknowledgements

This study has been supported by the National Natural Science Foundation of P. R. China (Grant No. 52005066) and State Key Laboratory of Mechanical Transmission (Grant No. SKLMT-KFKT-201706).

REFERENCES

[1] V. Simon, 1988, Load and stress distributions in spur and helical gears, Journal of Mechanisms, Transmissions and Automation in Design, 110, 197–202. https://doi.org/10.1115/1.3258926

[2] V. Simon, 2008, Influence of tooth errors and misalignments on tooth contact in spiral bevel gears[J]. Mechanism and Machine Theory, 43(10): 1253-1267. https://doi.org/10.1016/j.mechmachtheory.2007.10.012

[3] A. Kahraman, 1994. Load sharing characteristics of planetary transmissions. Mechanism and Machine Theory, 29(8), 1151–1165. https://doi.org/10.1016/0094-114x(94)90006-x

[4] H. Zedong, M. Ken, 2017, An investigation of misalignment effects on the performance of acetal gears. Tribology International, 116, 394-402. https://doi.org/10.1016/j.triboint.2017.07.029

[5] Kumar P., Hirani H., Agrawal A.K., 2019, Effect of gear misalignment on contact area: Theoretical and experimental studies. Measurement, 132, 359-368. https://doi.org/10.1016/j.measurement.2018.09.070

[6] L. Shuting, 2007, Effects of machining errors, assembly errors and tooth modifications on loading capacity, load-sharing ratio and transmission error of a pair of spur gears. Mechanism and Machine Theory,42, 698-726. https://doi.org/10.1016/j.mechmachtheory.2006.06.002

[7] L. Shuting, 2015, Effects of misalignment error, tooth modifications and transmitted torque on tooth engagements of a pair of spur gears. Mechanism and Machine Theory, 83, 125-136. https://doi.org/10.1016/j.mechmachtheory.2014.09.011

[8] L. Tengjiao, H. Zeyin, 2017, Analytical method for coupled transmission error of helical gear system with machining errors, assembly errors and tooth modifications. Mechanical Systems and Signal Process. 91, 167-182. https://doi.org/10.1016/j.ymssp.2017.01.005

[9] F. Mengjiao, M. Hui, L. Zhanwei, et al, 2018, An improved analytical method for calculating time-varying mesh stiffness of helical gears. Meccanica, 53, 1131-1145. https://doi.org/10.1007/s11012-017-0746-6

[10] W. Zhiguo, C. Hongrui, Z. Yanyang, et al, 2015, Mesh stiffness calculation using an accumulated integral potential energy method and dynamic analysis of helical gears. Mechanism and Machine Theory, 92, 447-463. https://doi.org/10.1016/j.mechmachtheory.2015.06.011

[11] W. Qibing, Z. Bo, F. Yang, et al, 2018, An improved time-varying mesh stiffness model for helical gear pairs considering axial mesh force component. Mechanical Systems and Signal Process, 106, 413-429. https://doi.org/10.1016/j.ymssp.2018.01.012

[12] M. Hui, P. Xu, Pang, F. Ranjiao, et al, 2015, Improved time-varying mesh stiffness model of cracked spur gears. Engineering Failure Analysis, 55, 271-287. https://doi.org/10.1016/j.engfailanal.2015.06.007

[13] H. Yifan, C. Kangkang, M. Hui, et al, 2019, Deformation and meshing stiffness analysis of cracked helical gear pairs. Engineering Failure Analysis, 95, 30-46. https://doi.org/10.1016/j.engfailanal.2018.08.028

[14] Saxena A., Parey A., Chouksey M., 2016, Time varying mesh stiffness calculation of spur gear pair considering sliding friction and spalling defects. Engineering Failure Analysis, 70, 200-211. https://doi.org/10.1016/j.engfailanal.2016.09.003

[15] H. Lin, Q. Houjun, 2017, Influences of tooth spalling or local breakage on time-varying mesh stiffness of helical gears. Engineering Failure Analysis, 79, 75-88. https://doi.org/10.1016/j.engfailanal.2017.04.017

[16] Sainsot P., Velex P., Duverger O., 2004, Contribution of gear body to tooth deflections-a new bidimensional analytical formula. Journal of Mechanical Design, 126, 748-752. https://doi.org/10.1115/1.1758252

Submitted: 13.8.2020

Accepted: 30.3.3021

Zeyin He
School of Mechantronics & Vehicle Engineering, Chongqing Jiaotong University No.66 Xuefu Road, Nan'an District, Chongqing 400074, China and State Key Laboratory of Mechanical Transmission, Chongqing University

Weiyi Tang
Department of Mechantronics engineering, Sichuan Vocational College of Information Technology
No.265 Xuefu Road, Li Zhou District, Guangyuan Sichuan 628040, China

Shizheng Sun
School of Mechantronics & Vehicle Engineering, Chongqing Jiaotong University
No.66 Xuefu Road, Nan'an District, Chongqing 400074, China